Journal of Theoretical Biology 268 (2011) 30–38

Contents lists available at ScienceDirect

Journal of Theoretical Biology

journal homepage: www.elsevier.com/locate/yjtbi

Pattern formation and chaos in spatial ecological public goods games

Joe Yuichiro Wakano [a,*], Christoph Hauert [b]

[a] Meiji Institute for Advanced Study of Mathematical Sciences, 1-1-1 Higashi Mita, Tama-ku, Kawasaki, Kanagawa 214-8571, Japan
[b] Department of Mathematics, University of British Columbia, 1984 Mathematics Road, Vancouver, BC, Canada V6T 1Z2

ARTICLE INFO

Article history:
Received 24 May 2010
Received in revised form
1 September 2010
Accepted 18 September 2010
Available online 1 October 2010

Keywords:
Spatial game theory
Cooperation
Maximum Lyapunov exponent
Reaction–diffusion system

Abstract: Cooperators and defectors can coexist in ecological public goods games. When the game is played in two-dimensional continuous space, a reaction diffusion model produces highly irregular dynamics, in which cooperators and defectors survive in ever-changing configurations (Wakano et al., 2009. Spatial dynamics of ecological public goods. Proc. Natl. Acad. Sci. 106, 7910–7914). The dynamics is related to the formation of Turing patterns, but the origin of the irregular dynamics is not well understood. In this paper, we present a classification of the spatio-temporal dynamics based on the dispersion relation, which reveals that the spontaneous pattern formation can be attributed to the dynamical interplay between two linearly unstable modes: temporal instability arising from a Hopf-bifurcation and spatial instability arising from a Turing-bifurcation. Moreover, we provide a detailed analysis of the highly irregular dynamics through Fourier analysis, the break-down of symmetry, the maximum Lyapunov exponent, and the excitability of the reaction-term dynamics. All results clearly support that the observed irregular dynamics qualifies as spatio-temporal chaos. A particularly interesting type of chaotic dynamics, which we call intermittent bursts, clearly demonstrates the effects of the two unstable modes where (local) periods of stasis alternate with rapid changes that may induce local extinction.

1. Introduction

Spontaneous and complex pattern formation represents a common principle not only in physical and chemical systems but also in biological systems (Gell-Mann, 1994; Pearson, 1993) or vegetation patterns in arid ecosystems (Rietkerk et al., 2004). Similar types of patterns emerge in evolutionary settings of social dilemmas, as shown in Fig. 1 (Wakano et al., 2009).

Social dilemmas are characterized by a conflict of interest between individuals and the group (Hauert et al., 2006b; Hardin, 1968), which arise in humans (Milinski et al., 2006, 2008) and microorganisms alike (Rainey and Rainey, 2003; Neu, 1992; Velicer and Yu, 2003). Humans are facing sustainable management challenges of global proportions when it comes to fisheries, fossil fuels or the climate (Ostrom, 1999) – each individual has the opportunity to make a small sacrifice for the benefit of all. Similarly, microorganisms can synthesize and secrete enzymes at some cost to get access to nutrients (Greig and Travisano, 2004) or to deactivate antibiotics (Neu, 1992), but this benefits others as well. Both scenarios are prone to exploitation because those that rely on everyone else's efforts do better – to the detriment of all. Such situations are captured by public goods games (Kagel and Roth, 1995; Hauert et al., 2006b).

In a typical public goods interaction, N individuals choose whether to contribute into a common pool or not. The total contributions are multiplied by a factor, $r>1$, and distributed equally among all participants. Hence, for $r<N$ defectors dominate but for $r>N$ it becomes advantageous to switch to cooperation (Hauert et al., 2006b). In well-mixed populations interaction groups are randomly formed according to binomial sampling and the evolutionary dynamics can be described by the replicator equation (Hofbauer and Sigmund, 1998), which predicts the demise of cooperators for $r<N$. However, this classic result neglects the fact that cooperator populations have a higher productivity than defector populations. This should be reflected in the natural assumption that cooperators are capable of maintaining higher population densities than defectors.

In ecological public goods games (Hauert et al., 2006a, 2008) the density of cooperators, u, and of defectors, v, can vary ($u+v\le 1$). The density dependent dynamics is captured by the following set of ordinary differential equations (ODE):

$$\dot{u} = u[w(f_C+b)-d],$$
$$\dot{v} = v[w(f_D+b)-d], \qquad \text{(ODE)}$$

where b denotes the baseline birth rate, d the death rate, $w=1-u-v$ the density dependent reproductive success and f_C, f_D represent the payoff for cooperators and defectors, respectively, for the details, see Appendix A and Hauert et al. (2006a, 2008). The average interaction group size is $\overline{S}=(u+v)N$. This introduces

* Corresponding author.
E-mail address: joe@math.meiji.ac.jp (J.Y. Wakano).

0022-5193/$ - see front matter © 2010 Elsevier Ltd. All rights reserved.
doi:10.1016/j.jtbi.2010.09.036

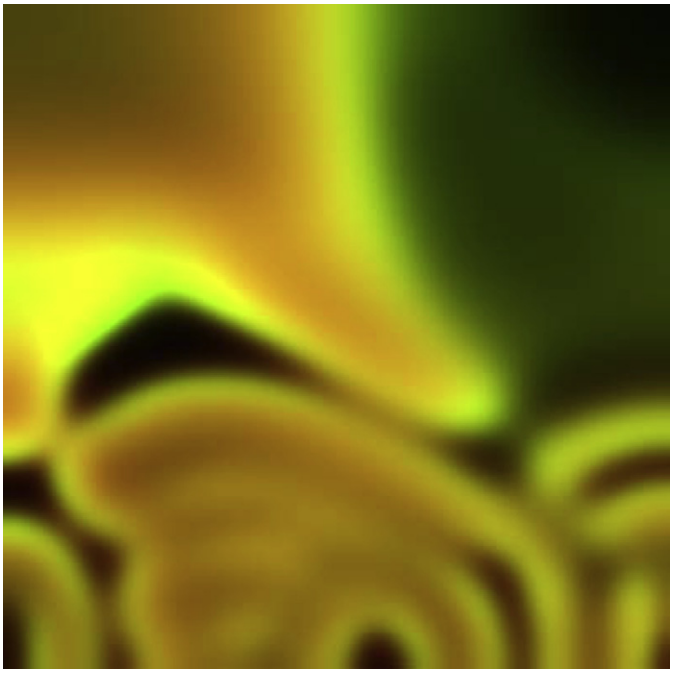

Fig. 1. A snapshot of irregular spatial dynamics in ecological public goods games. The color brightness indicates the density of cooperators (green) and defectors (red). Parameters: $r=2.35$, $D=3.6$, $b=1$, $d=1.2$, $N=8$, $t=8000$, $L=400$. (For interpretation of the references to color in this figure legend, the reader is referred to the web version of this article.)

a negative feedback between ecological dynamics and evolutionary games: If population densities are high, interaction group size, S, is large and defectors dominate. This reduces the average population payoff and hence leads to a decrease of the population density. As a consequence, S decreases but once $S<r$ holds, the social dilemma is relaxed and cooperators thrive, which increases the population density because of a higher average population payoff and results again in larger interaction groups and the cycle continues. In the following we focus on the more interesting case where the death rate exceeds the baseline birth rate ($d>b$) such that defectors cannot survive in the absence of cooperators ($\dot{v}<0$ for $u=0$).

This system admits rich dynamics including a Hopf-bifurcation and stable limit cycles (Hauert et al., 2008). However, truly fascinating dynamics unfold when including spatial dimensions and allowing individuals to migrate by adding a diffusion term to Eq. (ODE). Spatial extension favors the survival of cooperators if their diffusion rate is smaller than that of defectors. Therefore, cooperators do not outrun defectors but aggregate in clusters. The fast diffusing defectors readily locate thriving patches of cooperators but at the same time diffusion prevents defectors from efficiently exploiting those patches. This can result in the spontaneous formation of spatio-temporal patterns including highly irregular dynamics of ever changing patterns (Wakano et al., 2009).

Here we present a detailed analysis of the irregular dynamics based on dispersion relation, which reveals an interesting interplay between the dynamical instability arising from the Hopf-bifurcation of Eq. (ODE) and the Turing instability of the spatial system. Furthermore, we provide detailed evidence that the population dynamics exhibits spatio-temporal chaos in this regime.

2. Model

As a preparation for the discussion of the spatial dynamics let us briefly recall some important properties of the non-spatial

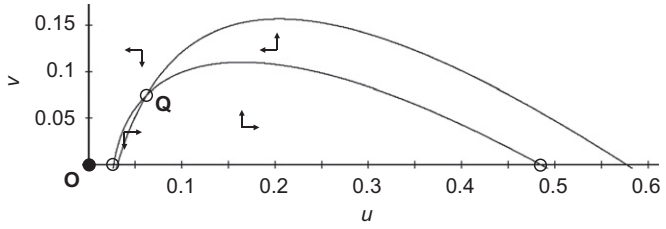

Fig. 2. Isoclines for u and v. Note that the u- and v-axes are also isoclines for v and u, respectively. The extinction equilibrium **O** is always locally stable and the two equilibria along the u-axis are always unstable. The internal equilibrium **Q**, $(u_Q,v_Q)=(0.062,0.075)$, is an unstable focus for $r<r_H\approx 2.3658$. Parameters: $r=2.34$, $b=1$, $d=1.2$, $N=8$.

dynamics (see Eq. (ODE)). First note that the dynamic does not admit chaotic solutions because it is a two-variable dynamical system. Second, under our assumptions ($1\le b<d$, $2<r<N$), the ODE admits two fixed points that are of particular interest: **O** and **Q**. The isoclines of the ODE are shown in Fig. 2. The state **O** denotes the extinction of the population ($u=v=0$) and is always locally stable. The existence and local stability of the internal equilibrium **Q**, where cooperators and defectors coexist, depends on the parameter values. Unfortunately, the coordinates of **Q**, (u_Q,v_Q), are not analytically accessible and hence the threshold parameter values are only numerically obtained. Taking r as a bifurcation parameter, the system exhibits a Hopf bifurcation at $r=r_H$. For $r>r_H$, **Q** is a stable focus. We can show (by calculating the first Lyapunov coefficient numerically) that the bifurcation is subcritical. This means that an unstable periodic solution exists for $r>r_H$ and that no (stable) limit cycle bifurcates from **Q** (for details see Hauert et al., 2008). Thus, the ODE asymptotically converges to either **O** or **Q** (if **Q** is locally stable). Numerically we confirm that **O** is globally stable for $r<r_H$ and that the system is bistable for $r>r_H$. The basin of attraction of **Q** increases with r but remains limited. No limit cycle is found.

2.1. Spatial model

Under the assumption that cooperators and defectors migrate randomly in a continuous two-dimensional space, the spatial dynamics is obtained by adding diffusion terms to Eq. (ODE), which results in the following reaction diffusion (RD) system:

$$\begin{aligned}\partial_t u &= D_C\nabla^2 u + u[w(f_C+b)-d],\\ \partial_t v &= D_D\nabla^2 v + v[w(f_D+b)-d]\end{aligned}\qquad\text{(RD)}$$

in a square domain $(x,y)\in[0,L]^2$ with zero-flux boundary conditions (see Appendix B). The functions $u(x,y,t)$ and $v(x,y,t)$ denote the density of cooperators and defectors at location (x,y) and time t. As before, $w=1-u-v$ determines the negative feedback between population density and birth rates. The diffusion coefficients D_C and D_D specify the migration rates for cooperators and defectors and ∇^2 denotes the diffusion operator. By rescaling space, we can choose the diffusion coefficient of cooperators to be unity such that

$$D_C=1,\quad D_D=D.$$

The system exhibits a wide variety of dynamics depending essentially on r and D.

3. Dispersion relation

Cooperators and defectors act as activators and inhibitors, respectively, and diffusion-induced instability (Turing instability)

occurs for sufficiently large D, i.e. if defectors diffuse faster than cooperators (Wakano et al., 2009). This result can be refined by classifying the dynamics according to the linear stability of the spatial model based on the dispersion relation. The dispersion relation links the wave number of a spatial perturbation and the corresponding eigenvalue. Small perturbations at the equilibrium **Q** given by $(u_Q+\delta u\cos k_1 x\cos k_2 y, v_Q+\delta v\cos k_1 x\cos k_2 y)$, grow or shrink according to $\delta u\sim\exp(\lambda(k)t)$ and $\delta v\sim\exp(\lambda(k)t)$ where $k^2=k_1^2+k_2^2$. The equilibrium is locally stable iff $\mathrm{Re}(\lambda(k))<0$ for all k. Since (u_Q,v_Q) are analytically inaccessible, the dispersion relation is derived numerically, see Fig. 3. In the region of interest, the dispersion relation has two peaks, $\mathrm{Re}(\lambda(0))$ and $\lambda(k^*)$: the first peak at $k=0$ (and hence termed *zero-mode*) refers to the instability of **Q** in the ODE and the second peak at k^* originates from Turing instability and is hence termed *Turing-mode*. For $r<r_H$ the equilibrium **Q** is unstable and reflected in a positive zero-mode, which indicates that the amplitude of temporal oscillations is increasing. If the Turing-mode is positive, spatial disturbances with the corresponding wavelength are amplified and grow exponentially as long as the system is well approximated by linearization, i.e. as long as the deviation from **Q** is small. Numerically we confirmed that the dispersion relation has at most two peaks for all parameter values.

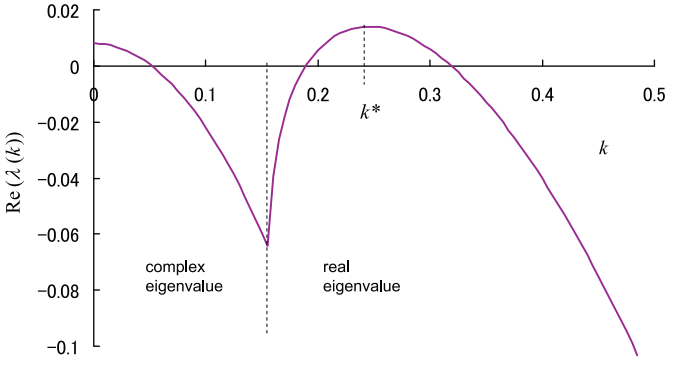

Fig. 3. Dispersion relation. Real part of the eigenvalue of the linearized system around **Q** is shown as a function of the wave number k of the spatial perturbation. For $r=2.34<r_H$ the zero-mode ($k=0$) has a complex eigenvalue with a positive real part. As k increases, the eigenvalues become real and the second peak appears at $k^*\simeq 0.245$, which corresponds to a wavelength of $l=25.1$. Parameters: $r=2.34$, $D=5$, $b=1$, $d=1.2$, $N=8$.

The Hopf bifurcation (ecologically induced instability) and the Turing bifurcation (diffusion-induced instability) can be used to classify the instability of the spatially homogeneous coexistence equilibrium $(u(x,y),v(x,y))=(u_Q,v_Q)$. Hereafter we denote by **Q** the corresponding spatially homogeneous solution of the spatial dynamics. The Hopf bifurcation turns **Q** into an unstable node for $r<r_H$ while Turing bifurcation makes **Q** unstable to spatial perturbations for $D>D_T(r)$. The threshold for Turing instability, $D_T(r)$, can be numerically obtained without calculating spatio-temporal dynamics (Wakano et al., 2009). For Turing instabilities it is often assumed that they develop in the vicinity of a *stable* equilibrium of the corresponding ODE, which would require $r>r_H$. Here we extend the domain of $D_T(r)$ to $r<r_H$ by defining that Turing-mode has zero eigenvalue when $(r,D)=(r,D_T(r))$. The two lines $r=r_H$ and $D=D_T(r)$ divide the parameter space (r,D) into four regimes, depending on the two types of instabilities, see Fig. 4.

The dynamics in the two regimes where $r>r_H$ holds are well understood (Wakano et al., 2009). Here we focus on the other two regimes ($r<r_H$), for which **Q** is unstable with respect to spatially homogeneous perturbations (zero-mode). This type of instability has been termed *ecologically induced instability* because it already exists for ecological dynamics in the absence of space (ODE). Without spatial heterogeneity, the population goes extinct. In a region where both diffusion- and ecologically induced instability exist, **Q** is unstable with respect to both types of perturbations. Since both zero-mode and Turing-mode grow, the dynamics may depend on the dominant mode. If zero-mode is dominant (i.e. $\mathrm{Re}(\lambda(0))\gg\lambda(k^*)$), global oscillations are expected to drive the population to extinction. If Turing-mode is dominant, spatial perturbations with stripes or spots should grow—at least at first. The growth of the Turing-mode is suppressed by the non-linearity of the system resulting in stationary patterns of stripes or spots. However, since the zero-mode is also unstable, it is not clear whether Turing patterns can indeed emerge and persist. Such global predictions based on a local analysis become particularly challenging whenever the instabilities of the two modes have similar magnitudes.

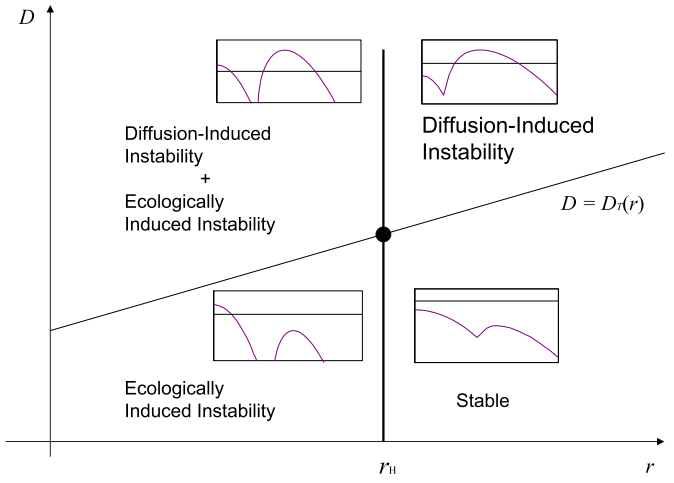

Fig. 4. Classification of instabilities. According to dispersion relation at equilibrium **Q** (shown in boxes), the parameter space (r,D) is divided into four regimes. The bold line marks the Hopf bifurcation while the thin line corresponds to the Turing bifurcation. The filled circle represents the Turing–Hopf bifurcation point at $(r_H,D_T(r_H))\simeq(2.3658,4.7)$.

3.1. Interplay between Turing-mode and zero-mode

Predictions based on the dispersion relation (Fig. 4) do not fully agree with the numerical results if the system displays ecologically induced instability. This is not too surprising because the dispersion relation applies in the vicinity of **Q** but for $r<r_H$ the amplitude of (temporal) oscillations around **Q** increase over time. This is reflected in the unstable zero-mode, $\mathrm{Re}(\lambda(0))>0$.

For a better understanding of the global dynamics under ecologically induced instability, let us consider three different cases with an unstable zero-mode. (i) In the absence of Turing instability ($D<D_T(r)$), the zero-mode is the dominant mode and an amplification of the temporal fluctuations results in extinction. (ii) In the other extreme, if the Turing-mode is much more unstable than the zero-mode, i.e. $\lambda(k^*)\gg\mathrm{Re}(\lambda(0))>0$ (or $D\gg D_T(r)$), the Turing instability is dominant and stationary patterns emerge—at least if r is not so small that the population goes extinct. The Turing instability seems to overrule the zero-mode instability resulting in the same kind of stationary patterns as in the regime of diffusion-induced instability ($r>r_H$). (iii) If the instabilities of the zero-mode and the Turing-mode are of similar

magnitude numerical results indicate that spatio-temporal chaos appears (see Section 4). The resulting dynamics is a combination of stabilizing spatial pattern formation (Turing-mode) and destabilizing temporal fluctuations (zero-mode), which we termed intermittent burst dynamics. For symmetrical initial configurations, spatial patterns form while temporal oscillations increase. Initially these oscillations are globally synchronized and eventually drive the population almost to extinction. Only small local patches survive, which then become sources for newly emerging spatial patterns. Over time the system loses its symmetry (see Section 4.1) and the global synchronization also disappears but locally synchronized oscillations persist. As a result, the spatial patterns in different regions oscillate with different phases (see supplementary Movie and Hauert, 2010). According to our numerical calculations, this irregular dynamic lasts at least for very long times. However, we cannot exclude that this represents a long-lasting transient that eventually leads to extinction. Decreasing D reduces the importance of the Turing-mode and the organizing principle of the Turing instability is no longer apparent (see Fig. 1).

The interaction (or interference) of diverging temporal oscillations (zero-mode) and organizing spatial pattern formation (Turing-mode) suggests that the line $\mathrm{Re}(\lambda(0))=\lambda(k^*)$ could indicate a threshold between stationary patterns if Turing-mode dominates and chaotic dynamics if the zero-mode dominates. This seems to apply in the vicinity of the Turing–Hopf-bifurcation but rapidly deteriorates for smaller r.

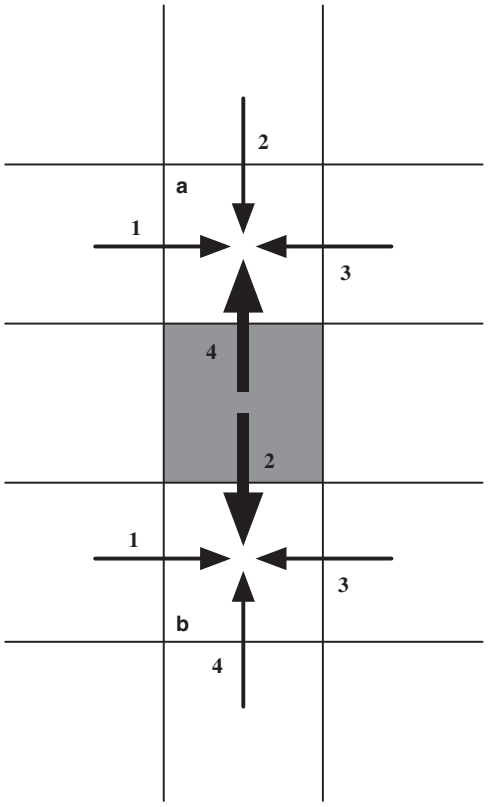

Fig. 5. Schematic illustration for the cause of the break-down of symmetry in numerical solutions of Eq. (RD). In the discretized system, consider a high-density cell (grey) surrounded by low-density cells (white) and compare the effects of diffusion into the cells **a** and **b**. If the numerical procedure first determines the flux from the adjacent cells in the sequence east, north, west, south, then for **a**, the first three summands are small, $o(\varepsilon)$, and the last one large, $o(1)$, yielding a sum of the form $\varepsilon+\varepsilon+\varepsilon+1$; but for **b** the second summand is large and the sum becomes $\varepsilon+1+\varepsilon+\varepsilon$. Due to numerical underflow the sums are not necessarily the same and the first one tends to be bigger than the second. In the regime of chaotic dynamics, the system is highly susceptible to small disturbances and hence these differences get amplified over time and eventually become sufficiently big to generate visible differences. The symmetry can be preserved at considerable cost in terms of CPU time by first sorting the summands. The sorting does not eliminate underflow errors but only ensures that they occur in a symmetrical manner.

4. Properties of chaos

Even though the dynamics *looks* highly irregular in time and space, it is usually impossible to actually *prove* that the dynamics exhibits spatio-temporal chaos. We have performed several analyses to provide strong evidence supporting that the dynamics in spatial ecological public goods games indeed can display deterministic chaos.

4.1. Symmetry break-down

Since Eq. (RD) is deterministic and the boundary conditions are symmetric, the solution must remain symmetric as long as the initial configuration is symmetric. However, the numerical integration of Eq. (RD) maintains the symmetry only for some time (kaleidoscopic patterns develop) but then irregularities become visible, spread quickly and the symmetry disappears (see supplementary Movie). The reason is that the accumulation of numerical errors does not occur in a spatially symmetric manner. For a schematic illustration of the detailed cause, see Fig. 5. At considerable expense in terms of computing time, this asymmetry can be removed (Fig. 6).

The numerical symmetry break-down is not merely a minor technical issue but implies that the smallest numerical errors grow rapidly and drastically change the global patterns. The susceptibility to small changes is one of the hallmarks of chaos. In Section 4.3 we demonstrate that the deviations actually grow exponentially, as required.

For many studies on pattern formation, such small spatial asymmetries are negligible. In fact, for models on the pattern formation of bacterial colonies, small perturbations in system parameters are even introduced to prevent symmetrical solutions and trigger pattern formation and, in particular, the branching patterns of interest (see e.g. Kawasaki et al., 1997; Mimura et al., 2000; Wakano et al., 2004).

4.2. Population dynamics

The local dynamics of the density of cooperators and defectors fluctuates heavily over time (see Fig. 7). The dynamics is dominated by oscillations around the unstable focus **Q**. However, no (stable) limit cycle exists because the Hopf bifurcation is subcritical. Instead, the dynamics keeps fluctuating with increasing amplitude, which results in the frequent local extinction of cooperators and defectors (see Fig. 7 and black regions in Figs. 1 and 6). However, local populations can recover and resume the oscillations around **Q** because of migrants from the neighborhood. Because extinction events are localized, spatial heterogeneity provides a source to repopulate vacant areas and hence prevents, or at least reduces the risk of global extinction. The global average of cooperator and defector densities equally oscillates around **Q** but with much smaller amplitude (data not shown).

Another hallmark of chaotic dynamics is given by the continuous power spectrum and the long tail of the time series (Weisbuch, 1991). The power spectrum of the local dynamics is shown in Fig. 8. The peak at period 52.5 corresponds to the dominant oscillations around **Q**. Note that this is in good agreement with expectations based on the linearized system around **Q**. The Jacobian matrix has complex eigenvalues of

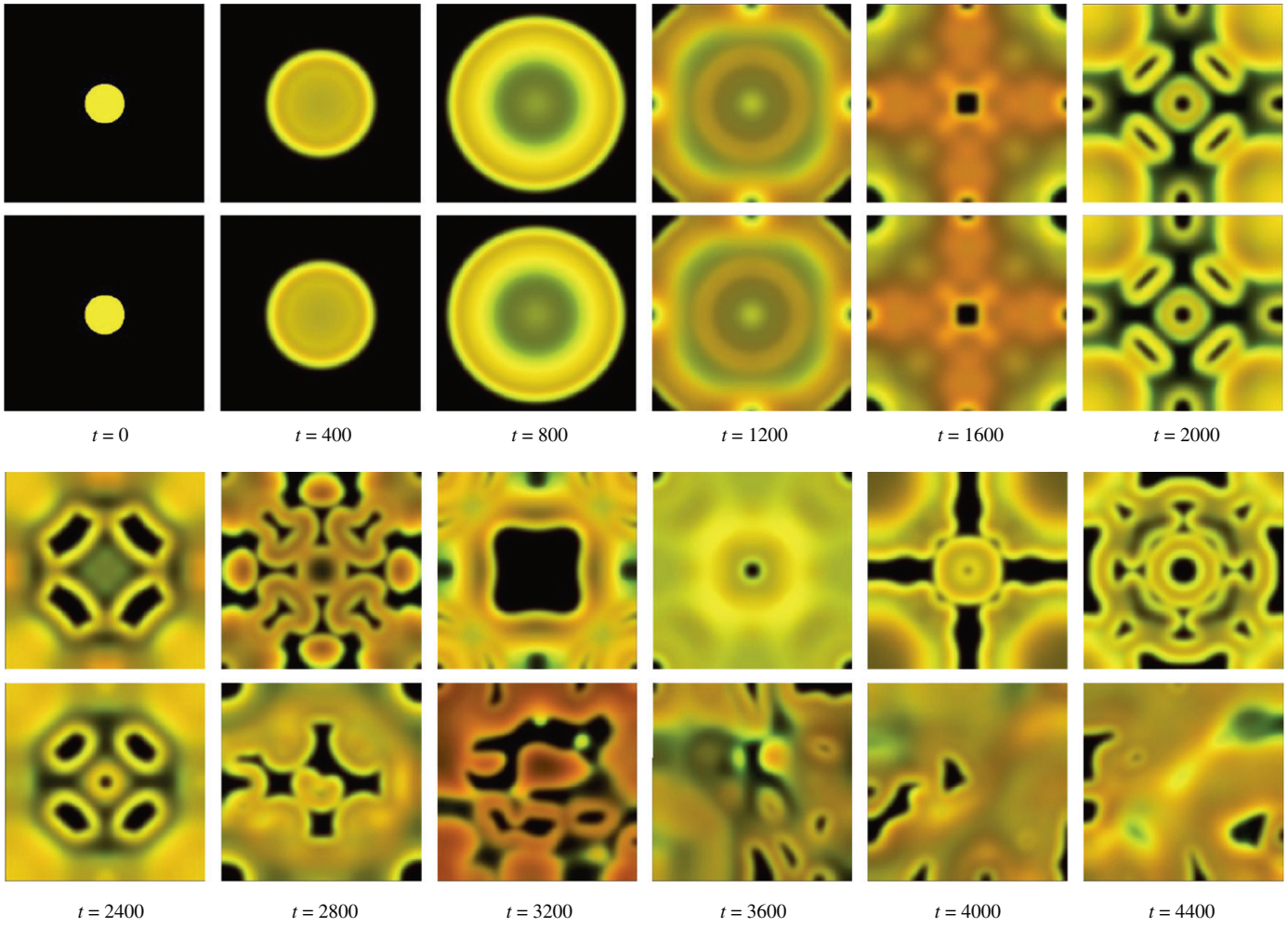

Fig. 6. Snapshots of the numerical solution of Eq. (RD) in the chaotic regime for symmetrical initial configurations: original algorithm (lower row) and modified algorithm with symmetry preserving counter measures (upper row). In the chaotic regime errors due to numerical underflow get amplified over time and eventually results in visible irregularities and the loss of symmetry (cf. Fig. 5). Parameters: $r=2.34$, $D=2$, $b=1$, $d=1.2$, $N=8$, $L=256$.

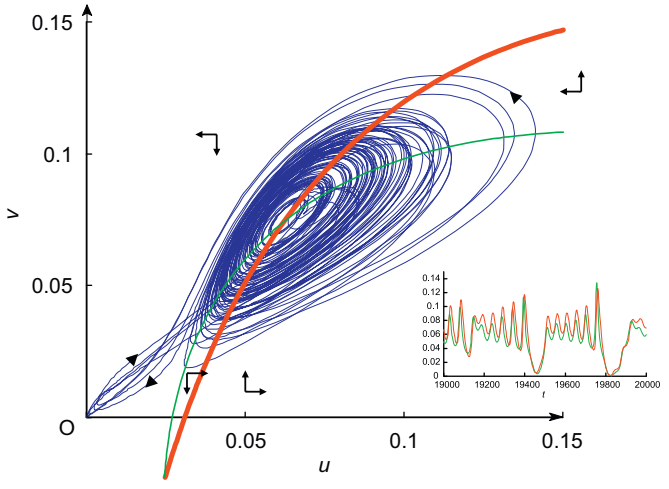

Fig. 7. Dynamics of the local density of cooperators and defectors. The trajectory in phase space for the local dynamics in the center of the two-dimensional space is shown together with the corresponding isoclines of the non-spatial system, Eq. (ODE). The inset depicts a short time series of the local densities of cooperators (green) and defectors (red). Parameters: $r=2.34$, $D=2$, $b=1$, $d=1.2$, $N=8$, $L=256$, relaxation time $t_R=15\,000$. (For interpretation of the references to color in this figure legend, the reader is referred to the web version of this article.)

$\lambda_{\pm}=0.008\pm0.135i$ and hence predicts oscillations with a period of $2\pi/0.135\approx46.5$.

4.3. Lyapunov exponent

The maximum Lyapunov exponent is one of the most commonly used indicators for deterministic chaos. The Lyapunov exponent measures the amplification of the distance between two initially close configurations. If the distance grows exponentially, the system exhibits chaos (see e.g. Schuster, 1995). The norm $|\mathbf{s}|$ of a spatial configuration – where $\mathbf{s}=(u(x,y,t),v(x,y,t))$ and $u(x,y,t)$, $v(x,y,t)$ denote the densities of cooperators and defectors, respectively – is given by

$$|\mathbf{s}|^2=\int_0^L\int_0^L u(x,y,t)^2+v(x,y,t)^2\,dy\,dx \tag{1}$$

on the two-dimensional domain $(x,y)\in[0,L]^2$ where L represents the linear extension of space. The distance between two configurations $\mathbf{s}_1$, $\mathbf{s}_2$ is then simply $|\mathbf{s}_1-\mathbf{s}_2|$. Let $\mathbf{s}(t)$ and $\mathbf{s}_\varepsilon(t)$ be the solution of Eq. (RD) with slightly different initial configurations $\mathbf{s}(0)=\mathbf{s}_R$ and $\mathbf{s}_\varepsilon(0)=\mathbf{s}_R+\varepsilon$, respectively. The maximum

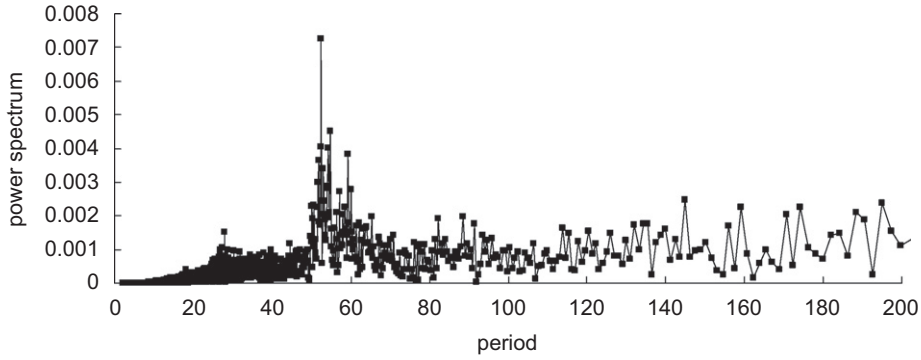

Fig. 8. Power spectrum of the time series generated by the local dynamics of cooperator density. The spectrum has a clear peak at period 52.5, which corresponds to the oscillations around **Q**. The spectrum is continuous with a long tail and hence provides further support for chaotic dynamics. The initial transient data is omitted in the time series. Parameters: $r=2.34, D=4, b=1, d=1.2, N=8, t=3000-20\,000$.

Table 1
Typical maximum Lyapunov exponents for the different dynamical regimes.

r	D	λ ($t=3000$)	λ ($t=4000$)	Spatial dynamics
2.34	100	−0.0026	−0.0028	Diffusion-induced coexistence (stationary)
2.34	4	+0.1794	+0.2378	Diffusion-induced coexistence (intermittent burst)
2.34	2	+0.1426	+0.1653	Diffusion-induced coexistence (chaotic)
2.50	100	−0.0016	−0.0018	Diffusion-induced instability (stationary)
2.50	2	−0.0431	−0.0431	Homogeneous coexistence (stationary)

Lyapunov exponent, λ, given by

$$\lambda=\lim_{t\to\infty}\frac{1}{t}\ln\frac{|\mathbf{s}(t)-\mathbf{s}_\varepsilon(t)|}{|\varepsilon|}. \tag{2}$$

However, note that the distance between two configurations is bounded and hence it is not possible to take the limit $t\to\infty$ (because then $\lambda\to 0$). In practice, we calculate

$$\lambda(\mathbf{s}_R,\tau)=\max_\varepsilon\left\{\frac{1}{\tau}\ln\frac{|\mathbf{s}(\tau)-\mathbf{s}_\varepsilon(\tau)|}{|\varepsilon|}\right\} \tag{3}$$

that is the Lyapunov exponent at reference state $\mathbf{s}_R$ (see Appendix C for detail).

Note that in the special case where the reference state corresponds to the stationary homogeneous density distribution the growth or decline of spatial perturbations is captured by the dispersion relation (see Section 3).

Typical maximum Lyapunov exponents for the different dynamical regimes are listed in Table 1 and illustrated in Fig. 9. The maximum Lyapunov exponent for stable spatially homogeneous coexistence is -0.0431, which is consistent with the zero-mode eigenvalue $-0.0425\pm 0.186i$. All Lyapunov exponents are negative for stationary patterns and positive for irregular patterns, which supports that this regime exhibits spatio-temporal chaos.

4.4. Excitable system

Another important feature of our system is its 'excitable' reaction term. For $r<r_H$, the ODE system inevitably converges to the extinction state **O**. However, the trajectories are very different for different initial points. To illustrate this, we plot the time to extinction, i.e. the time required for the system to converge to the close vicinity of **O** as a function of the initial point $(u(0),v(0))$ (see Fig. 10). If r is slightly smaller than r_H, trajectories stay near **Q** for a long time if the initial point is near **Q**. Furthermore, we observe separatrix originating from an unstable equilibrium (saddle) on the u-axis. This divides the phase space into two regions: If the initial point lies to the left, the system quickly approaches **O** but if the initial point lies to the right, the dynamics results in a burst of cooperation followed by an increase of defectors, before the system eventually goes to extinction. Thus, even though the asymptotic behavior is independent of the initial state, the transient behavior can be markedly different: Small perturbations of the extinction state **O** vanish quickly but perturbations of appropriate size and direction can trigger the system to 'fire', i.e. excite the system. Our system is more easily excited if the perturbation consists of more cooperators and less defectors. In spatial settings diffusion can act as the source of such perturbations. Indeed, high-density clusters of cooperators (green) invade empty space (black). The invasion excites the local dynamics so that the cooperator density quickly grows and generates opportunities for defectors to exploit, which then – after some oscillations – leads back to local extinction. During the time lag between local excitation (invasion) and local extinction, cooperators and defectors co-exist and through migration (diffusion) they can excite neighboring areas. Thus, if new excitations are triggered before local extinction, the population can survive.

5. Discussion

Spatial ecological public goods games can give rise to a brave new world of pattern formation (Wakano et al., 2009). The emergence of static patterns is well understood based on Turing instabilities. However, Turing instabilities alone are not sufficient to explain the particularly intriguing dynamical regime of highly irregular spatio-temporal patterns. Based on the dispersion relation we provide a detailed analysis of this regime and show that the dynamics results from an interplay between the Turing instability and ecological instability arising from the Hopf-bifurcation (Hauert et al., 2008). Emerging spatial heterogeneity (Turing instability) actually stabilizes the system by reducing the chances that the population is driven to extinction. Conversely, ecological instability tends to induce increasing oscillations that can result in (local) extinction. These two competing forces are responsible for the irregular dynamics and we provide strong evidence that the irregularity actually arises from deterministic chaos. Most notably by suggesting a numerical technique to determine the maximum Lyapunov exponent in spatial systems.

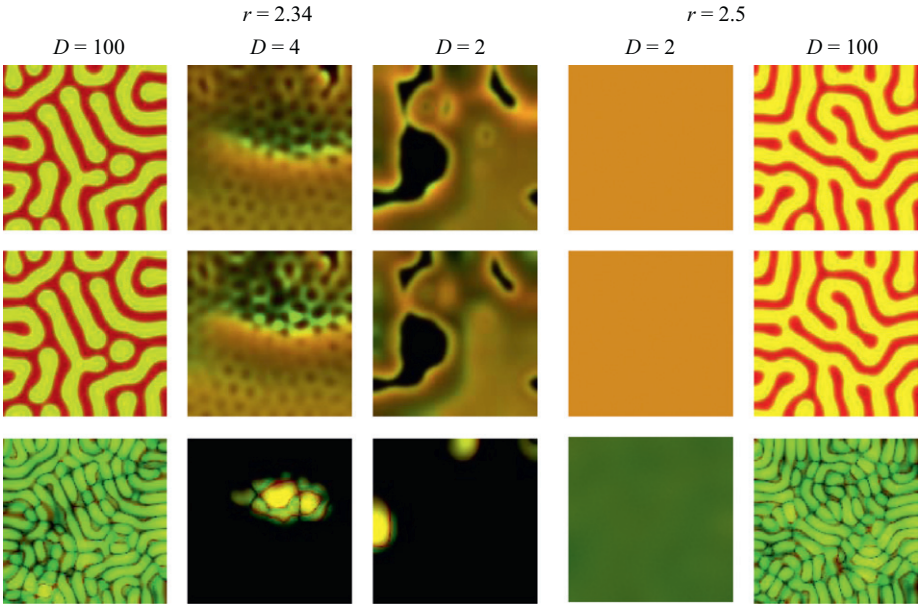

Fig. 9. Reference states at $t=t_R$ (upper) and at $t=t_R+\tau$ (middle), and the corresponding deviation vector ε that gives maximum Lyapunov exponents (bottom). We do not show the state at $t=t_R+\tau$ with deviation because the difference is indistinguishable. See Table 1 for the corresponding Lyapunov exponents. Parameters: $b=1$, $d=1.2$, $N=8$, $t_R=3000$.

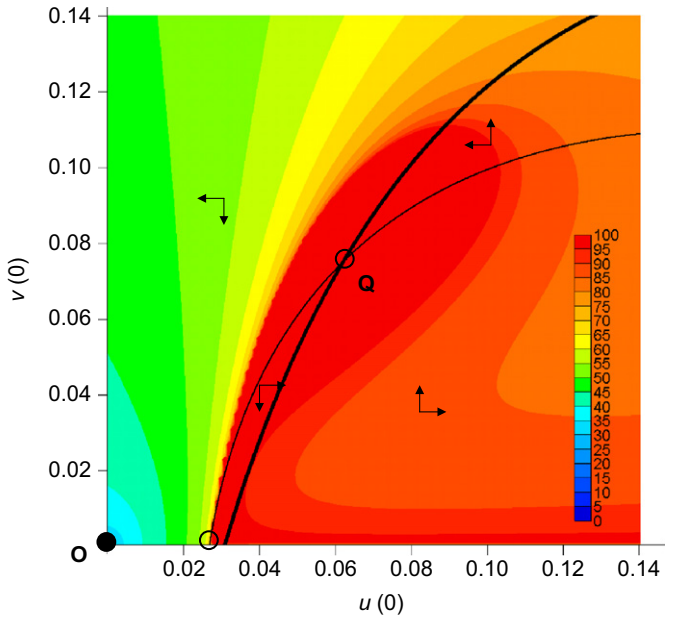

Fig. 10. Time to extinction without spatial structure for various initial values $(u(0),v(0))$, shown with isoclines. When the system experiences a large perturbation at the extinction state **O**, it sometimes takes relatively long time to return there. The dynamics has a single global attractor **O** but the system is excitable. Parameters: $r=2.34$, $b=1$, $d=1.2$, $N=8$.

Spatial structure supports cooperation because it enables cooperators to form local clusters. This is most apparent in typical lattice or graph structured populations (Nowak and May, 1992; Hauert, 2001; Ohtsuki et al., 2006; Szabó and Fáth, 2007). Discrete space and discrete density facilitate cluster formation and segregation of cooperators and defectors. Even in the absence of interactions, clusters form simply because reproduction is local (cf. the vast literature on the voter model, Liggett, 1991). In fact, game interactions may either enhance or inhibit this inherent tendency of cooperators to form clusters (Hauert and Doebeli, 2004). This is very different in models with continuous space and continuous densities, such as reaction–diffusion systems. Clustering is no longer a built-in characteristic unless we consider advection terms such as success-driven motion (Helbing, 2009). In reaction–diffusion system, the density of defectors is positive everywhere and cooperation cannot evolve even when cooperators are clustered in the initial distribution (Wakano, 2006).

In general, diffusion flattens heterogeneous distributions but under special circumstances diffusion interferes with the reaction dynamics and can give rise to pattern formation. These famous Turing patterns can be interpreted as a mechanism for spontaneous cluster formation. Such clusters are not a built-in property of reaction–diffusion models but occur only if migration and game dynamics 'cooperate'. The key to the formation of cooperative clusters is diffusion-induced instability: Turing patterns meet spatial game theory.

Acknowledgements

We thank Masayasu Mimura and Kota Ikeda for valuable comments. J.Y.W. is partly supported by JST PRESTO and by JSPS KAKENHI No. 20770019. C.H. acknowledges support by the Natural Sciences and Engineering Research Council of Canada (NSERC).

Appendix A. Derivation of payoff functions

An individual interacts in a group of size S with probability

$$Pr[S]=\binom{N-1}{S-1}(1-w)^{S-1}w^{N-S},$$

where N denotes the number of sampling trials and w indicates the probability that a trial failed and did not add another participant. An individual in a group of size S faces m cooperators and $S-1-m$ defectors among its $S-1$ co-players with probability

$$Pr[m|S]=\binom{S-1}{m}\left(\frac{u}{u+v}\right)^{m}\left(\frac{v}{u+v}\right)^{S-1-m}$$

and it gets the benefit from the investment by the m cooperators. Thus, a defectors payoff equals mr/S and a cooperator receives $mr/S+r/S-1$, which accounts for the costs of cooperation and the return from its own investment. Thus, defectors and cooperators in a group of size S receive the following expected payoffs

$$P_D(S)=\frac{r}{S}\sum_{m=0}^{S-1} mPr[m|S],$$

$$P_C(S)=P_D(S)+\frac{r}{S}-1.$$

Averaging over all possible group sizes S, we obtain

$$f_i=\sum_{S=2}^{N} Pr[S]P_i(S)$$

with $i=C$ or D. Here we assume that the payoff is zero if an individual is the only member of its group (i.e. $S=1$). Thus, the average payoffs for defectors, f_D, and cooperators, f_C, are given by

$$f_D=r\frac{u}{1-w}\left(1-\frac{1-w^N}{N(1-w)}\right), \tag{4a}$$

$$f_C=f_D-F(w), \tag{4b}$$

where

$$F(w)=1+(r-1)w^{N-1}-\frac{r}{N}\frac{1-w^N}{1-w}. \tag{4c}$$

Appendix B. Numerical setup

For the numerical solution of our spatial model, we use three different methods: explicit Euler method, implicit Cranck–Nicholson method with ADI (alternating direction implicit), and finite element method (Press et al., 1988; Hecht et al., 2005) and confirm that the different numerical algorithms produce qualitatively the same result. We also confirm that the different domain shapes produce qualitatively similar results (Wakano et al., 2009). The linear system size, L, is chosen so that L is large enough to include multiple unstable spatial wavelengths. Preliminary calculations show that the spatial dynamics is little affected by the initial configurations, which makes a clear contrast with ODE dynamics. We have studied various kinds of initial configurations but here we mainly show the results for two types: either a disc at the exact center of the spatial domain in which cooperators and defectors co-exist ($u=v=0.1$) or a random distribution where the densities of cooperators and defectors are randomly determined by a uniform distribution in [0,0.1]. The disc pattern is used to investigate the transient dynamics and otherwise a random pattern is used.

Appendix C. Calculation of maximum Lyapunov exponent

The spatial domain is discretized as an $n\times n$ square lattices. Each lattice point (i,j) represents a point $(iL/n,\ jL/n)$. This discretization turns our partial differential equation Eq. (RD) with two species (cooperators and defectors) into a set of $2\times n\times n$ ordinary differential equations. Thus, each spatial configuration $\mathbf{s}=(u_{ij},v_{ij})$ corresponds to a $2n^2$-dimensional vector. The norm of $\mathbf{s}$ is defined as

$$|\mathbf{s}|=\sqrt{\sum_{i=1}^{n}\sum_{j=1}^{n}(u_{ij}^2+v_{ij}^2)}.$$

In order to determine the maximum Lyapunov exponent, we apply the following algorithm:

1. Let the system develop into chaotic dynamics (or a stationary pattern if no chaos appears). After relaxation time t_R, we obtain a reference state $\mathbf{s}$.
2. Choose a $2n^2$-dimensional deviation vector ε with each of its components randomly chosen from [0,1]. Then normalize ε so that $|\varepsilon|=0.1$.
3. Calculate spatio-temporal dynamics starting from $\mathbf{s}$ for time τ. Define the result as $\mathbf{s}'$.
4. Calculate spatio-temporal dynamics starting from $\mathbf{s}+\varepsilon$ for time τ. Define the result as $\mathbf{s}'_\varepsilon$.
5. Let k be the ratio of the norm of the difference $|\mathbf{s}'_\varepsilon-\mathbf{s}'|$ to the norm of the initial difference $|\varepsilon|=0.1$. Formally,
$$k=\frac{|\mathbf{s}'_\varepsilon-\mathbf{s}'|}{|\varepsilon|}.$$
6. Normalize the deviation vector, i.e. set a new ε as
$$\varepsilon=\frac{\mathbf{s}'_\varepsilon-\mathbf{s}'}{k}.$$
7. Repeat steps 4–6 for m times.

During the iteration, the deviation vector ε aligns with the most unstable direction indicated by the eigenvector to the eigenvalue with the largest real part, which maximizes the deviation $|\mathbf{s}'_\varepsilon-\mathbf{s}'|$. The maximum Lyapunov exponent λ for the reference state $\mathbf{s}$ is approximated by

$$\lambda=\frac{1}{\tau}\ln k,$$

where k represents the final value after the iteration. Numerically we find that 20 iterations ($m=20$) are sufficient to obtain consistent results. In the chaotic regime the magnitude of Lyapunov exponent may depend on the reference state $\mathbf{s}$. Therefore the Lyapunov exponent was calculated for two different reference states at $t_R=3000$ and 4000. In Table 1 and Fig. 9, the initial configuration is a random distribution.

Appendix D. Supplementary data

D.1. Supplementary movie

Intermittent burst dynamics. The movie is encoded in H.264 format and requires Quick Time 7 or higher. It merges 2000 JPEG images, which are available from the author upon request. Parameters: $r=2.34, D=4, b=1, d=1.2, N=8, t=0-8000, L=256$.

Supplementary data associated with this article can be found in the online version at doi:10.1016/j.jtbi.2010.09.036.

References

Gell-Mann, M., 1994. The Quark and the Jaguar: Adventures in the Simple and the Complex. W. H. Freeman & Co, New York, NY.
Greig, D., Travisano, M., 2004. The Prisoner's Dilemma and polymorphism in yeast SUC genes. Biol. Lett. 271, S25–S26.
Hardin, G., 1968. The tragedy of the commons. Science 162, 1243–1248.
Hauert, C., 2001. Fundamental clusters in spatial 2×2 games. Proc. Roy. Soc. London B 268, 761–769.
Hauert, C., 2010. Virtuallabs: interactive tutorials on evolutionary game theory ⟨http://www.univie.ac.at/virtuallabs⟩.

Hauert, C., Doebeli, M., 2004. Spatial structure often inhibits the evolution of cooperation in the snowdrift game. Nature 428, 643–646.
Hauert, C., Holmes, M., Doebeli, M., 2006a. Evolutionary games and population dynamics: maintenance of cooperation in public goods games. Proc. Roy. Soc. London B 273, 2565–2570.
Hauert, C., Michor, F., Nowak, M., Doebeli, M., 2006b. Synergy and discounting of cooperation in social dilemmas. J. Theor. Biol. 239, 195–202.
Hauert, C., Wakano, J.Y., Doebeli, M., 2008. Ecological public goods games: cooperation and bifurcation. Theor. Popul. Biol. 73, 257–263.
Hecht, F., Pironneau, O., Le Hyaric, A., Ohtsuka, K., 2005. Freefem++ 3.8.0: finite element method to solve partial differential equations 〈http://www.freefem.org〉.
Helbing, D., 2009. Pattern formation, social forces, and diffusion instability. Eur. Phys. J. B 67, 345–356.
Hofbauer, J., Sigmund, K., 1998. Evolutionary Games and Population Dynamics. Cambridge University Press, Cambridge.
Kagel, J.H., Roth, A.E. (Eds.), 1995. The Handbook of Experimental Economics. Princeton University Press, Princeton.
Kawasaki, K., Mochizuki, A., Matsushita, M., Umeda, T., Shigesada, N., 1997. Modeling spatio-temporal patterns generated by bacillus subtilis. J. Theor. Biol. 188, 177–185.
Liggett, T.M., 1991. Stochastic Interacting Systems: Contact, Voter and Exclusion Processes. Springer.
Milinski, M., Semmann, D., Krambeck, H.-J., Marotzke, M., 2006. Stabilizing the earths climate is not a losing game: supporting evidence from public goods experiments. Proc. Natl. Acad. Sci. USA 103, 3994–3998.
Milinski, M., Sommerfeld, R., Krambeck, H.-J., Reed, F., Marotzke, J., 2008. The collective-risk social dilemma and the prevention of simulated. Proc. Natl. Acad. Sci. 105 (7), 2291–2294.
Mimura, M., Sakaguchi, H., Matsushita, M., 2000. Reaction–diffusion modelling of bacterial colony patterns. Physica A 282, 283–303.
Neu, H.C., 1992. The crisis in antibiotic resistance. Science 257, 1064–1073.
Nowak, M.A., May, R.M., 1992. Evolutionary games and spatial chaos. Nature 359, 826–829.
Ohtsuki, H., Hauert, C., Lieberman, E., Nowak, M.A., 2006. A simple rule for the evolution of cooperation on graphs and social networks. Nature 441, 502–505.
Ostrom, E., 1999. Governing the Commons. Cambridge University Press, Cambridge.
Pearson, J.E., 1993. Complex patterns in a simple system. Science 261 (5118), 189–192.
Press, W.H., Teukolsky, S.A., Vetterling, W.T., Flannery, B.P., 1988. Numerical Recipes in C. Cambridge University Press, Cambridge.
Rainey, P.B., Rainey, K., 2003. Evolution of cooperation and conflict in experimental bacterial populations. Nature 425, 72–74.
Rietkerk, M., Dekker, S.C., de Ruiter, P.C., van de Koppel, J., 2004. Self-organized patchiness and catastrophic shifts in ecosystems. Science 305, 1926–1929.
Schuster, H.G., 1995. Deterministic Chaos: An Introduction. Wiley-VCH Verlag, Weinheim.
Szabó, G., Fáth, G., 2007. Evolutionary games on graphs. Phys. Rep. 446, 97–216.
Velicer, G.J., Yu, Y.T.N., 2003. Evolution of novel cooperative swarming in the bacterium *Myxococcus xanthus*. Nature 425, 75–78.
Wakano, J.Y., 2006. A mathematical analysis on public goods games in the continuous space. Math. Biol. Sci. 201, 72–89.
Wakano, J.Y., Komoto, A., Yamaguchi, Y., 2004. Phase transition of traveling waves in bacterial colony pattern. Phys. Rev. E 69, 051904.
Wakano, J.Y., Nowak, M.A., Hauert, C., 2009. Spatial dynamics of ecological public goods. Proc. Natl. Acad. Sci. USA 106, 7910–7914.
Weisbuch, G., 1991. Complex Systems Dynamics. Addison-Wesley, Reading MA.